

## VOLCANICA Article in Press

- This is an uncorrected proof, meaning that this manuscript has not been copyedited or formatted according to Volcanica's styles and standards. In turn, this means that article content, including text, may still change prior to final publication. Although articles in press do not have all bibliographic details available yet, they can be cited using the year of online publication and the DOI, as follows: author(s)(year), article title, Volcanica, DOI.
- 5
- 10 Rader, E. et al. (2026) "Impact of an arctic environment emplacement on the surface glass content of the Lost Jim lava flow in the Imuruk Lake volcanic field, Alaska", Volcanica, 9(1). doi: 10.30909/vol/hvex3566.

# Relating glassy rind thicknesses to ambient air temperatures at the Lost Jim flow field in the Imuruk Lake volcanic field, Alaska: a preliminary report

15

Erika Rader<sup>1</sup>, Jessica Larsen<sup>2</sup>, Tim Orr<sup>3</sup>, Dawn Ruth<sup>3</sup>, Jessica Stanley<sup>1</sup>


<sup>1</sup> University of Idaho

<sup>2</sup> University of Alaska Fairbanks, Geophysical Institute and Department of Geosciences


20 <sup>3</sup>U.S. Geological Survey


\*erader@uidaho.edu

 ORCID (Rader): [0000-0001-8205-3461](https://orcid.org/0000-0001-8205-3461)

 ORCID (Larsen): [0000-0003-1171-129X](https://orcid.org/0000-0003-1171-129X)

 ORCID (Orr): [0000-0003-3695-9558](https://orcid.org/0000-0003-3695-9558)

25  ORCID (Ruth): [0000-0001-9369-9364](https://orcid.org/0000-0001-9369-9364)

 ORCID (Stanley): [0000-0001-8463-9271](https://orcid.org/0000-0001-8463-9271)

**Keywords:** Climate proxy, vitric rind, lava cooling rate, pāhoehoe, Mars

## Abstract

30 **The Lost Jim flow field, in the Imuruk Lake volcanic field, Alaska,** extends west ~34 km from a single vent, crossing subarctic tundra and currently touches several lakes and streams. The weighted mean of five <sup>36</sup>Cl cosmogenic exposure ages from the Lost Jim pāhoehoe flow is  $7.73 \pm 0.37$  ka, indicating this eruption occurred substantially after the eruption of the underlying Camille flow, which was emplaced at  $39.7 \pm 1.3$  ka. Paleoclimate records indicate the period when the Lost Jim flow field was emplaced was after deglaciation, and the climate was similar

35 to today. We propose that the emplacement of lava in these cold subarctic conditions can lead to faster cooling of the lava surface compared to lava emplaced in warmer locations such as mid-latitude cold deserts. Glass abundance in the outermost rinds at the Lost Jim flow field was on average 74% with 6.4 mm thick rims, compared to 60% with 2.9 mm rims for cold mid-latitude desert samples. We interpret increased glass content as a proxy for rapid cooling likely occurring partly during winter. Glassiness values varied less across vent, margin, and mid-

40 flow locations when compared to the mid-latitude flows suggesting the Lost Jim flow field was broadly impacted by the subarctic climate as opposed to responding to local microclimates. Our results indicate that lava glassiness may be a useful environmental indicator of cooler (in this case subarctic) conditions

## Introduction

The outermost portion of a cooling lava flow will experience, and respond to, the conditions of the environment in which it is emplaced. If this response is substantial, reliable, and repeatable, then it would be possible to infer environmental factors at the time of emplacement from the state of the rind of an old lava flow. The scientific literature supports a substantial and reliable impact of glassy rind formation in sub-aqueous lava flows, but little has been done to explore the variety of cooling environments that may influence rind formation on lava flows. We present an evaluation of rind qualities from a subarctic lava flow which suggests that further investigation into lava cooling processes could be fruitful for studying past weather and climate conditions.

**Lava cooling mechanisms** – Lava flow surfaces are cooled via radiative heat loss and convective cooling as fluids (air or water on Earth) move across the surface (Griffiths 2000, Keszthelyi & Denlinger 1996, Head & Wilson 1986). Radiative cooling dominates the initial drop in temperature as the heat loss is exponentially large when the lava is the hottest (Head & Wilson 1986). Given that the only variable in radiative cooling between two lava flows on the same planet is the difference in their starting temperature, the impact of this component of heat loss is likely to be very similar between environments. However, cooling by convection can be heavily influenced by the surrounding environment—notably, exposure to wind and water can greatly increase the cooling rate of flow surfaces by changing  $h$ , the convective heating coefficient (Keszthelyi et al 2003, Harris & Rowland 2001). Even the presence of snow and ice in contact with any side of the flow (under, on top, or beside) can cool the top of a lava flow faster, either by direct contact with meltwater dripping onto the flow or steam plumes blowing against the surface from margin contact (Edwards et al. 2014, 2015). However, interaction with snow or ice is likely to lead to distinctive cooling joint systems in the lavas and should be readily recognisable (Mee et al., 2009 Edwards et al. 2015, 2016). One environmental factor that impacts convective cooling rate is the ambient atmospheric temperature; yet, this is less studied, as the change is smaller and, on the scale of cooling an entire flow field, the impact is small (Patrick et al. 2004, Hirashima 1952). However, decreasing the ambient air temperature does increase heat flux, having an effect that would be most concentrated on the outermost surface. Thus, in a setting where two identical lava flows were cooling in different thermal environments, the outer rind of the lava flow in the colder environment would experience a faster cooling rate (Rowland et al. 2004). Sufficient studies to assess the magnitude of this impact on glass formation have not been conducted; however, if we assume

that small changes in cooling rate can influence the outermost surface of a flow, then these external environmental factors, including ambient temperature, may be responsible for differences in surface rim characteristics.

75

**Glassiness related to emplacement environment** –The impact of faster cooling and rind formation has not yet been studied at various air temperatures, but a more extreme example—lava-water interactions—can be useful for considering the outcome of colder ambient temperatures. The connection between water-influenced emplacement and lava glassiness is well established, with increased cooling rates leading to thicker glassy rinds (Keszthelyi & Denlinger 1996). Lava that interacts with abundant water, such as undersea eruptions, develops rind several cm thick (Nichols et al. 2009, Wilding et al. 2000, Wilding et al. 1996, Wilding et al. 1995). Flows that encounter water sources even minimally will develop a visibly glassy rind that is 25% thicker than air-cooled lavas (Lescinsky & Fink, 2000, Deschamps et al. 2014). Additionally, the presence of distinctive cooling joints will enable such environmental settings to be readily recognised. However, the cut off of where these features stop forming has not been constrained. One account suggested that heavy rain during lava emplacement led to a thicker glassy rind (Macdonald 1953), and another noted thick glassy rinds on pāhoehoe flows that interacted with snow (Edwards et al. 2015). The thickness of rind has also been shown to be influenced by non-hydrous cooling-enhanced environments, such as those that are windy (Keszthelyi et al. 2003, Keszthelyi & Denlinger 1996). The thermal responsiveness of the outermost rind of a pāhoehoe lobe suggests that environmental conditions such as very low air temperatures, in addition to the presence or absence of water or wind, can influence glass content. However, the extent and conditions of this sort of cooling is not known. Cooling occurs in numerous stages from magma chamber to final equilibrium with the emplacement environment (Reeder et al. 2024). For example, small crystals may grow in the conduit during ascent or in the lava during flow at the surface. Thus, it is important to assess the quality of the glass microscopically when using crystallinity and glassiness as a proxy for cooling rate. We investigate two aspects of glassiness, both the rind thickness and the crystal content of the outermost 50 microns of the rind, to examine what differences emplacement environment might have on the sample overall.

Further, additional factors such as melt viscosity and mechanical erosion during and after emplacement can influence the rind formation and preservation. Erosion rates on young lava flows in dry locations with no visible erosion have been assumed to be 0—1 mm/ky in geochronological studies, so pristine surfaces were presumed to have rind thickness that were close to original (Fenton et al. 2014, Marchetti et al. 2014, Heinicke et al. 2016). Crystal kinetics and the glass forming ability of a lava must also be considered, since undercooling and degassing may increase polymerization in higher-silica melts (>57 wt. % SiO<sub>2</sub>), causing suppressed nucleation and thus fewer

crystals at slower cooling rates (Iezzi et al. 2008, Vetere et al. 2015). To control for this, studies examining glass  
105 content of lava flows should consider the chemical composition of the lava as well as any stagnation/ponding that  
may have occurred on the flow field, thus allowing further crystallization during emplacement.

Previous studies on Holocene basaltic lava flow rinds indicate that glass distribution across the surface of pāhoehoe  
flows can range from 20% to 100%, which is partly due to variable thermal microenvironments (Rader et al. 2022,  
110 Reeder et al. 2024). For example, vent material can either be very glassy from rapid quenching during flight or  
have very little glass due to oxide crystal growth resulting from prolonged exposure to high- temperature gases  
(Rader et al. 2022). Additionally, lava samples collected from the flow surface in the middle of a flow field (mid-  
flow) are generally glassier than samples collected from the outermost flow margins, although a good mechanism  
for this has not yet been identified (Reeder et al. 2024). Thus, a broad range of sample locations is important to  
115 consider all these environments when attempting to characterize the overall cooling environment a lava flow  
experienced. Lava flows in the Rader et al. 2022 and Reeder et al. 2024 studies are located in the inland northwest  
USA between 41° and 43° (mid-) latitude at 1300—1700 meters elevation, erupted into a similar dry cold desert,  
and are similar bulk compositions (basalt). Thus, they provide a distinct group to compare with flows emplaced in  
colder environments to assess the effect that latitude (i.e., climate) has on emplacement conditions. They are  
120 referred to as desert mid-latitude comparison flows. Further exploration into the variability of glass abundance  
across lava flow fields requires a wider range of emplacement environments than what is captured in these two  
previous studies.

**Lost Jim lava flow and Camille lava flow** – The two youngest flows in the Imuruk Lake Volcanic Field are both  
125 basaltic flows that were generated in an extensional tectonic setting and have not produced confident  
geochronological ages previously. The Lost Jim lava flow (65.4876, -163.2969) is a basaltic lava thought to be  
younger than the last glacial maximum (Hopkins 1968), although absolute dating has proven difficult. The lava  
was too young to be resolved by  $^{40}\text{Ar}/^{39}\text{Ar}$  dating (Mukasa et al. 2007), whereas a  $^{13}\text{C}$  date of 1655 ybp of organic  
material from beneath an ash layer of unknown provenance near the flow field has confounding uncertainties  
130 (Hopkins 1988, Kaufman and Hopkins 1985). Further uncertainty surrounds the impact the subarctic environment  
had on the morphology of the flow field with “collapse” pits that had been attributed to subsurface melting of  
permafrost by the lava flow (Begét et al. 2008, Marcucci et al. 2017). However, a recent analysis of the flow  
morphology suggests that permafrost collapse was wrongly implicated as the cause of the pits across the surface of  
the flow (Orr et al. 2025). Nevertheless, the subarctic emplacement environment of the Lost Jim flow field may

135 have been substantially colder than the mid-latitude desert flows. Additionally, abundant surface water is found in lakes, streams, and perched on the tundra during the short summer, whereas ice and snow cover the region during the winter, all of which would increase cooling rates on lava flow surfaces (Hopkins 1959, Patrick et al. 2004, Edwards et al. 2014, 2015). There are no classic indicators of lava-water interaction such as hackly jointing, palagonite formation, pillow structures, or explosive deposits at Lost Jim flow field, indicating that water was not  
140 a dominant cooling mechanism. However, it is relevant to note the degree to which moisture is present, as this differs significantly from the desert comparison group. Surface morphology is dominated by inflated pāhoehoe with transitional morphologies lining only a few narrow channels, suggesting most of the lava was insulated from the environment until shortly before emplacement; thus the environment in the location of final emplacement is more likely to have influenced the cooling rate than changes during transport. To confirm the likelihood of a  
145 subarctic environment during emplacement given that climate has changed over time, we used  $^{36}\text{Cl}$  to provide exposure dates for the flow.

The second youngest flow, the Camille flow, was also sampled in the hopes these samples could provide additional glass data; however, the surface was so disrupted from frost wedging that determining primary surfaces was challenging and too few samples were collected to be utilized for the glass study. We do, however, report the  $^{36}\text{Cl}$   
150 dates for the underlying Camille flow to evaluate the timescales responsible for the extensive frost wedging across the flow. We surveyed the glass content of the rinds across a wide variety of lava surfaces at Lost Jim flow field to evaluate the potential impact that environmental factors may have had on the cooling history of the lava flow.

## Methods and materials

155 **Field:** Helicopter-supported field work allowed for the collection of 23 lava and spatter samples across the flow field for petrographic analysis (Fig. 1). The lava samples were predominantly from intact pāhoehoe surfaces, but two samples were from rubbly parts of the flow (LJ21-19 and 20). Sites were selected for their emplacement environment based on previous study results that indicate microenvironments may influence cooling rate (e.g. wet margin, vent, mid-flow), and samples were chosen to have intact, fresh surface textures exhibiting minimal erosion  
160 or weathering (Fig. 2, Table 1). Vent samples included intact and broken spatter surfaces, which were only selected if they had a coherent rind that resembled a flow surface and were not oxidized. Mid-flow samples were lava surfaces that were at least 20 meters away from the furthest marginal extent of the flow. Margin samples were collected within 5 meters along the furthest extent of the flow, with ‘dry’ samples showing no evidence of current water influence. Samples collected from ‘wet margins’ means substantial water existed at the margins at the time

165 of sampling, not necessarily that water was present at the time of eruption (Reeder et al. 2024, Rader et al. 2024).  
As lava flows can impound surface water after cooling, it is possible that modern-day ‘wet’ margins may not have  
been in direct contact with water at the time of eruption. However, as the chances of water being present at the time  
of emplacement is greater in these locations than in the ‘dry’ locations, there may have been a different influence  
on the cooling history or weathering history of the glass; thus, the current presence of water is noted for each  
170 sample. The only hornito sampled was a small rootless spatter pile located over a lava tube and unrelated to lava-  
water interactions. An additional eight samples from Lost Jim and Camille lava flows were collected for  
cosmogenic dating; we required thin and flat samples with an intact surface, with little shadowing from surrounding  
micro- and macro-topography.

175 **<sup>36</sup>Cl exposure geochronology:** <sup>36</sup>Cl exposure dating is a method that has been successfully used to date young  
basaltic rocks (e.g. Downs et al. 2021, Parmelee et al. 2015, Vazquez and Woolford 2015, Zreda et al. 1993). In-  
situ <sup>36</sup>Cl dating is based on the production of <sup>36</sup>Cl near the surface of the Earth due to the interaction of cosmogenic  
particles with Ca, K, Ti, Fe, and Cl in rocks. Calibrated production rates of <sup>36</sup>Cl can then be used to calculate the  
surface exposure age of a sample using the measured concentrations of <sup>36</sup>Cl and the sample geochemistry. The  
180 eight samples we collected for this purpose were surface slabs 6—9 cm thick and whole sample was processed  
instead of isolated mineral separates due to the fine-grained nature of the materials. Samples were sent to the Purdue  
University Rare Isotope Measurement (PRIME) Laboratory, Indiana, USA, for dissolution and measurement of  
<sup>36</sup>Cl. Dissolved whole rock separates were spiked with <sup>35</sup>Cl and concentrated. Cl isotopes were then measured using  
accelerator mass spectrometry. We calculated ages of the flows from <sup>36</sup>Cl concentration and sample geochemistry  
185 using the CRONUScalc v2.1 web interface (Marrero et al. 2016, Marrero et al. 2021). We used the cosmogenic  
production rates of Lal (1991) and Stone (2000) by selecting the ‘Lm’ scaling framework within CRONUScalc,  
which accounts for time variability in the strength of the magnetic field (Marrero et al. 2016a). We assumed post-  
eruption erosion of the samples to be negligible based on the observation of the apparent youthfulness of volcanic  
surface features (e.g. fresh glassy surfaces, minimal lichen growth, and poor soil development on the surface).  
190 There also was no correlation between lava flow age and rim thickness, suggesting erosion was not a dominant  
process (Supplemental Materials). Topographic shielding was also assumed to be negligible as samples were taken  
from prominent horizontal surfaces and the local topography is relatively flat (see Orr et al. 2025 for more  
discussion of flow morphology). We used a bulk density of 2.8 g/cm<sup>3</sup> and an attenuation length of 160 g/cm<sup>2</sup>.  
Whole rock major oxide and trace element data used in the calculations were acquired from Washington State  
195 University’s (WSU) Peter Hooper Geoanalytical laboratory as part of a forthcoming companion study. Procedures

for X-ray fluorescence analyses (XRF; major oxide data) and inductively coupled plasma mass spectrometry methods (ICP-MS; trace element data) are available from Knaack et al. (1994), and Johnson et al. (1999), respectively. Analytical precision for whole rock major and trace element data collected via the WSU Geoanalytical laboratory is discussed in Nye et al. (2018). The full input table used to make the calculations can be found in  
200 Supplemental Table 1.

**Petrographic analysis:** Hand samples were cut perpendicular to the surface to capture the change in texture from rind to interior and made into thin sections (Fig. 3). In addition to examining the thickness of the rind, the number of crystals preserved in the outermost rind (~50 microns) was also measured. Eight to ten backscattered electron  
205 images were collected of the rind portion of the thin section with the Tescan Vega3 scanning electron microscope housed at the U.S. Geological Survey Menlo Park (now Moffett Field), California, USA. Instrument conditions were set uniformly for all images collected. The accelerating voltage and working distance were set to 20 kV and 13 mm, respectively. Brightness and contrast were manually adjusted to optimally capture the observed textures. Magnification was set at 200x (FOV = 3.2 mm) for most images and increased to 600x (FOV = 1.08 mm) when  
210 necessary to observe fine textures.

Crystal modal percentage was calculated for each image using the program ImageJ (Schneider et al. 2012) to count the number of pixels (a proxy for crystal content) of each phase for glass, olivine, plagioclase, iron oxides, and vesicles (Rader et al. 2022, Reeder et al. 2024). The starting crystal content was used to control for crystal growth  
215 during transport or stagnation. For samples with >9% vesicles, the total glass value as reported in tables 1 and 2 was calculated as the percent of the total minus the vesicle area. Thickness of glass rinds was also measured from thin sections magnified by 10x from the edge of the sample to the depth where the groundmass color turned from dark brown to black/opaque in plane polarized light as crystals become too thick to allow light to pass. The boundary between opaque and dark brown glass was distinct in all samples with rinds greater than 1 mm in  
220 thickness.

**Comparative mid-latitude desert site selection** – We compiled (Table 2) the modal percent of glass and rind thickness data from 31 previously published lava samples from volcanic fields in Oregon and Idaho, USA. These include samples from Jordan Craters, analyzed by Reeder et al. (2024), and samples from Blue Dragon Flow,  
225 Diamond Craters, The Devil's Garden, Four Craters Lava Field, and Hells Half Acre, analyzed by Rader et al.

(2022). Geochemically, all samples are basalt or trachy-basalt with SiO<sub>2</sub> values ranging from 47—52 wt. % and total alkali values between 3.09 and 5.75 wt. %. The full geochemical analyses can be found in their respective publications and in supplemental table 2. These samples all come from lava flows erupted in Cold Semi-Arid or Cold Desert regions, or BSk/BWk in the Köppen-Geiger climate classification (Beck et al. 2018). Mean annual temperatures of these sites are 5—10 °C, with mean winter minimum and summer maximum temperatures ranges of 5 to 0 °C and 20 and 28 °C, respectively (Arguez et al. 2010). When compared to the Imuruk Lake volcanic field's Köppen-Geiger subarctic classification, Dfc where the coldest month averages below 0 °C but at least three months have an average above 10°C, the lavas from Oregon and Idaho were more likely to experience warmer temperatures and less precipitation/surface water. Bulk compositions of samples in this study are plotted against glass characteristics in the supplemental data and indicate the variability in the samples in this manuscript do not correlate with any aspect of geochemistry.

## Results

**<sup>36</sup>Cl Ages and timescale of eruption** - Calculated ages for the Lost Jim flow ranges from 6.80±1.37 ka to 8.85 ± 2.1 ka, while the Camille flow ranged from 37.52 ± 6.97 ka to 43.56 ± 8.23 ka (1σ uncertainties including both analytical and production rate uncertainties, Table 3). This results in a weighted mean age of 7.73 ± 0.37 ka and 39.7 ± 1.3 ka, respectively for those two flows (1σ including the analytical uncertainties only).

The duration of the Lost Jim eruption can be crudely estimated using its volume. Hopkins (1963) proposed a total volume of 3.3—4.2 km<sup>3</sup>, which is 2—3 times the size of the 2014—2015 eruption of Holuhraun (1.44 km<sup>3</sup>), in Iceland. The Holuhraun eruption was emplaced in about 6 months; however, the surface morphologies (tube-fed inflated pāhoehoe) at the Lost Jim flow indicate lower effusion rates than those at Holuhraun (channelized transitional morphologies; Voigt et al. 2021). This suggests that the Lost Jim flow erupted on a time scale of years, and cooling rates were thus likely influenced by temperature variations over several seasonal cycles. As an unknown portion of the Camille flow is buried, no assessment was made to the duration or seasonality of this flow.

**Glass content of rinds**- The surface of the Camille flow was too degraded to ensure a robust sample of the original surface and so the thickness of the rind from the Camille samples are not included in this dataset. Although it is worth noting that despite the high degree of erosion on the surface of the Camille flow, two of the three collected samples still preserved some glassy rind, indicating the rind must have been thicker than the amount of erosion

which as occurred. The modal percent of glass for the 23 Lost Jim flow field samples ranged from 60—95% with an average of  $74\% \pm 8\%$  (Table 1). No systematic difference in crystallinity percentage was noticed that might indicate vast differences in starting crystal content upon emplacement. Of the vesicle-free area, the remainder of the percentage was crystals of plagioclase, which was usually 2—4 times more abundant than olivine. No samples  
260 contained measurable oxides and only the three samples nearest the vent (LJ21-07, 08, and 24) contained large numbers of vesicles that required correction as described in the methods. The average thickness of the rind of all the samples was  $6.4 \text{ mm} \pm 4.3 \text{ mm}$  with a range from 0.2 to 15.4 mm and a median value of 7 mm (Fig. 4). Pyroclastic morphologies contained the most modal percentage of glass (vent scoria 82% and hornito spatter 95%), whereas margins and mid-flow samples all contained very similar amounts of glass (averages between 72% and  
265 74%, Table 4, Fig. 5). Samples from dry margins had the highest average rind thickness (7.2 mm), followed by those from wet margins (6.5 mm), vent scoria (6.2 mm), and mid-flow samples (4.7 mm). The hornito sample had a glass rind of 4.3 mm.

The modal percent of glass for the 31 desert samples ranged from 24% to 82% with an average of  $60\% \pm 17\%$   
270 (Table 2). The average rind thickness was  $2.9 \text{ mm} \pm 3.1 \text{ mm}$ , with a range from 0.2 to 9.3 mm and a median value of 0.3 mm (Fig. 4). In these mid-latitude comparison samples, the highest modal percent glass content, at 78%, was found in a single hornito sample, and the lowest, at 53%, was found in vent spatter samples (Table 3, Fig. 5). Mid-flow samples, at 74%, were similar to the single wet margin sample (72%) but higher than the dry margin samples (58%). Rind thickness was highest in the mid-flow samples at 7.1 mm, followed by scoria (4.0 mm) and dry margins  
275 (2.7 mm). The wet margin sample has a rind thickness of 0.3 mm.

## Discussion

**Lava flow field ages-** Our  $^{36}\text{Cl}$  age for the Lost Jim flow field of  $7.73 \pm 0.37 \text{ ka}$  is significantly older than the previously hypothesized minimum age of  $1655 \pm 220$  years (Kaufman and Hopkins, 1985) but significantly younger  
280 than the age of the Camille flow at  $39.7 \pm 1.3 \text{ ka}$ . The age for the Camille flow confirms the hypothesis that it erupted during a period of glaciation but is older than was thought previously (Middle as opposed to Late Wisconsin) (Hopkins 1963). Further, the surface erosion of the Camille flow provides a potential age constraint on the preservation potential of glassy rinds, (e.g., flows in the 10s of thousands of years old should not be expected to retain original rinds). Although the cause for the erosion may have been the transition from glaciated period to  
285 non-glaciated opposed to age and hence rinds may be present if extensive frost wedging in an older flow is not

observed.

The previous age for the Lost Jim flow field comes from  $^{13}\text{C}$  dates of organic material extracted from beneath an ash layer of unknown provenance on the north side of Imuruk Lake (Kaufman and Hopkins 1985). The authors  
290 hypothesized that the ash came from the Lost Jim eruption; however, an explosive plume that produces ash-sized particles but no other explosive features, such as a caldera (Dzurisin et al. 1995, Freundt & Schmincke 1995) is uncommon for effusive basaltic eruptions nor is it consistent with the products that might be expected from the explosive eruption of low-viscosity basalt, such as Pele's hair and tears produced by fountaining. Further, the distribution of the ash does not match a pattern expected from an eruption at the Lost Jim vent (e.g., none near the  
295 Lost Jim vent and too thin at the location sampled).

One environmental variable that can impact the  $^{36}\text{Cl}$  date is persistent snow cover, which can attenuate cosmogenic particles and reduce the cosmogenic production rate of  $^{36}\text{Cl}$ . We did not account for this effect as it is difficult to estimate snow cover over geologic time. However, the nearest SNOTEL monitoring station (Pargon Creek, ~60  
300 km south of Imuruk Lake) indicates that for the past 24 years between the months of November and May there is usually between 22—26 cm of snow (United States, USDA 2025). A study on  $^{36}\text{Cl}$  ages at Mt. Erebus calculated that this amount of snow would impact the ages less than the analytical error of the measurement itself (Parmelee et al. 2015).

305 ***Climate during Lost Jim eruption*** - Given the  $^{36}\text{Cl}$  ages, we must consider the climate during 6,000—10,000 ybp, which is after the end of the last glacial maximum. During that time, the Imuruk Basin was ice-free but was very cold and windy (Hopkins 1963). Modern-day weather conditions are an acceptable proxy, as average temperatures were within half a degree of modern values for the region between 6,000 and 10,000 ybp (Herzschuh et al. 2023, Colinvaux 1962). The mean annual temperature in Kotzebue, Alaska, site of the weather station closest  
310 to the Lost Jim flow, was  $-5\text{ }^{\circ}\text{C}$  over the period from 1981—2010, which is the extent of that dataset. As Kotzebue is coastal and Imuruk Lake is interior as well as 310 meters higher in elevation, this temperature is likely warmer than that experienced by the eruption. A mean of  $-5\text{ }^{\circ}\text{C}$  compares to a mean annual temperature of  $5\text{—}10\text{ }^{\circ}\text{C}$  for our comparison group of mid-latitude flows (Arguez et al. 2010). Mean summer maximum and winter minimum temperatures are  $15\text{ }^{\circ}\text{C}$  and  $-8\text{ }^{\circ}\text{C}$  for Kotzebue, respectively, and range from  $20\text{ to }28\text{ }^{\circ}\text{C}$  and  $-5\text{ to }0\text{ }^{\circ}\text{C}$  for the mid-  
315 latitude sites. Given the volume estimate and the timescale of the Lost Jim eruption, the flowing lava experienced both the cold, windy conditions during the 7—8 months of winter as well as the swampy, thaw lake-covered tundra

during the brief cool summer (Hopkins, 1959). Thus, it is reasonable to assume the cooling environment during emplacement of most of the Lost Jim flow included a combination of cold, snowy, icy, wet, and windy conditions.

320 **Glass Distribution on the Lava surface** – The quenched rinds from all samples from the top of the Lost Jim  
flow field tend to have, on average, 14% more glass than the mid-latitude flows measured for this study.  
Additionally, the least glassy sample from the Lost Jim flow field was the same percentage as the average of the  
desert comparison group (60%). A t-test indicated that all the samples in the two groups are significantly different  
with p values < 0.001. It is possible that samples with less glassy rinds could be found at the Lost Jim flow field if  
325 targeted sampling was conducted; however, methods for sample collection were the same between all field sites,  
suggesting that the difference between the different latitudes is not due to sampling bias. The thickness of the glassy  
rinds from the Lost Jim flow extends, on average, twice as deep as the comparison group, indicating that the crust  
of the Lost Jim flow cooled faster than typical cold desert air-cooled lava flows. Rind thickness (fig. 4) varies more  
in the Lost Jim flow field samples, showing that, even in subarctic conditions, a very thin glassy rind may form, as  
330 some samples may be erupted during a warm portion of a day with no wind during the summer or protected from  
the harsh weather by microtopography.

The modal % glass content of the Lost Jim flow samples was highest for unoxidized pyroclastics, which is similar  
for our comparison group. However, unlike the desert lava samples, the difference in glass content at the margins  
335 and the middle of the Lost Jim flow did not vary greatly, indicating that the main control on cooling was likely the  
cold air temperature rather than environmental conditions that would have a bigger impact on the margins (e.g.  
shallowly ponded water). This also suggests that while a universal mechanism for the difference in margin and  
mid-flow glass contents for the comparison group is not known, the differences in cooling environment between  
these locations in the comparison group were greater.

340 Glassy rind thickness for the Lost Jim samples also tended to be greater than the mid-latitude samples in all the  
emplacement locations except mid-flow (fig. 5). In general, the samples with higher glass contents had thicker  
visible glassy rinds; however, there is a lot of variability within the samples, indicating that slight differences in  
the cooling environment may be influencing these two measures of glass content (rind thickness and modal % of  
345 glass). Our data set does not contain enough samples to do further statistics on what other aspects of the samples  
might be correlating with the variability. Our findings suggest that glass distribution in intact, unaltered lava flow  
surfaces records cooling histories that reflect the emplacement environment. Flow fields that have a continuous

glass content of ~70% along their margins may have experienced enhanced cooling from a colder environmental temperature or persistent wind, whereas discontinuous glassy margins may indicate brief or local surface water interaction during emplacement.

**Glassiness as an indicator for emplacement environment** - The thickness of the glassy rind on the surface of a lava flow, as well as the rind's modal percentage of glass, may reflect environmental conditions that produce faster cooling rates. However, it is important to note that the impact of climate and seasonality can overlap with shorter-duration flows. Our dataset compares the Lost Jim flow field to six other lava flows; all erupted in unknown weather conditions. Extreme weather (e.g. cold snaps, freezing rain, monsoons, blizzards) during an eruption may be the cause for some of the glassiness in the desert mid-latitude control group. An additional factor that could lead to thick glassy rinds in mafic lavas regardless of environmental conditions includes overpressurization or stagnation inside an inflated lobe, which allows for either resorption of vesicle gas or degassing and a subsequent densification of the glassy outer rind of the subsequent breakout (Oze & Winter 2005, Kauahikaua et al. 2003, Sage 2000). Thus, if utilizing this method, it is important to consider the location of the sample you are collecting. For example, margin and mid-flow samples are more likely than vent samples to be influenced by environmental conditions while cooling. Likewise, a few samples may not be enough to indicate a broad cooling environment, since samples air-quenched in any climate can end up highly glassy. Instead, a wide variety of samples should be assessed, and outliers evaluated for microenvironmental impacts, such as emplacement in a sheltered or insulated area, a clastogenic origin, or emplacement near a heat source, like a fumarole. Additionally, glassy rinds that do not have vesicles should be treated with caution in paleoenvironmental studies, as these thick rinds are attributed to lava flow dynamics instead of the local environment. Further study could help to understand the relationship between glass rind thickness, petrographic textures, and microlite growth and to better interpret emplacement environments and to understand the sensitivity lava flows may have to climate-related cooling.

Lava rinds must be preserved sufficiently (not physically weathered, though altered is acceptable if rind thickness is still distinct as can be the case for palagonitization) for an accurate assessment of the cooling environment during emplacement; thus, this method may not be as widely applicable to basaltic environments as hoped. However, glassy rinds have been found to be preserved in lavas 10—100s of millions of years old, such as the Deccan Traps, Columbia River Flood Basalts, and the Paraná Flood Basalts (Duraiswami et al. 2001, Bondre & Hart 2004, Waichel et al. 2006). Volcanically active locations that lack other paleoclimate records, such as small islands with no lakes, coral reefs, or glaciers, may benefit from this sort of climate information. This method, which requires no

analytical capabilities beyond magnification, could be applied to other planetary surfaces with volcanic activity or impact, to constrain regional or temporal changes in climate without the need for isotopic analysis.

## Conclusions

We provide the first geochronological dates for the Lost Jim flow, which erupted  $7.73 \pm 0.37$  ka, and the Camille flow, which erupted  $39.7 \pm 1.3$  ka. Despite emplacement of the Lost Jim flow being substantially after the last glacial maximum, the climate at that time was cold and windy, similar to today. The Lost Jim flow field, with an estimated volume of  $\sim 4$  km<sup>3</sup>, was probably emplaced on the timescale of years as opposed to months, necessitating some portion of the eruption occurring during the subarctic winter. The impact of the emplacement of the Lost Jim flow field during cold subarctic conditions may have influenced the formation of the glass content of the outermost rind of samples collected from across the flow field. The overall modal percentage of glass on a microscopic scale was greater than lava flows emplaced in the mid-latitude United States (74% vs 60%, respectively), with Lost Jim flow field samples extending to higher values. The thickness of the glass rind measured from standard 30  $\mu$ m thick petrographic thin sections was also greater (6.4 mm to 2.9 mm). The pattern of glassiness at the Lost Jim flow field generally follows that seen at other flows, with hornito spatter and unoxidized vent scoria having the highest glass contents, and glass contents of mid-flow samples being higher than those of margin samples. However, Lost Jim flow field samples exhibited less variability between the mid-flow and margin environments, suggesting cooling rates may have been buffered by a widespread factor, such as colder average temperatures, as opposed to water along the margins of the flow. Even though the weather during emplacement for the comparison desert lava flows is unknown, and each desert location is capable of overlap in extreme temperatures, moisture content, and wind magnitude, the cumulative evaluation of the glassiness of those samples suggests slower cooling times for the outer rinds of the mid-latitude lava flows. This study illustrates how measures of glassiness of the surface rind on an unaltered and largely intact lava flow may form in response to subarctic temperatures during lava flow emplacement, providing an additional temperature proxy for volcanically active areas. Lava flows with thick glassy rinds in places with few climate records could indicate time periods with significantly colder temperatures. Conversely, thin glassy rinds across a flow field may indicate a warmer climate at the time of emplacement. This relationship may be particularly important for locations such as Mars, where sedimentary rock paleoclimate data are limited, but lava flows are abundant and widespread (Tanaka et al. 2014). Lava rind thickness analysis could also help extend climate records on small volcanically active, terrestrial islands which lack other climate proxies such as lake sediment or ice core records. Further study to understand the broad application of this technique could

be beneficial, as the impact of numerous other factors, such as flow thickness, was not compared between flows,  
410 and because the hypothesized environmental conditions at the time of emplacement were not measured. However,  
the differences in glassiness shown in this paper suggests that a wider study that includes flows from more climates  
and observations of small-scale emplacement environments with collected samples of modern eruptions may allow  
for a broader application of this finding.

## 415 **Author contributions**

Erika Rader conceived of the project, obtained funding, conducted field work, analyzed the majority of the SEM  
and petrographic images, and wrote the majority of the first draft text and figures. Jessica Larsen and Tim Orr  
participated in field work and field discussions and provided whole rock geochemical data for the geochronology  
models. Dawn Ruth imaged the petrographic slides with the SEM and slide scanner for glass content analysis.  
420 Jessica Stanley interpreted the <sup>36</sup>Cl data and contributed to the first draft text. All authors edited the manuscript.

## **Acknowledgements**

Funding for this project was provided by NASA PSTAR award 80NSSC18K1518. Field work coordination and  
support was provided by the Alaska Volcano Observatory. Samples were collected under the National Park Service  
425 permit BELA-2021-SCI-0003. Modal % calculations for ¼ of the SEM images were completed by Owen Carswell  
to fulfil a workstudy position. Any use of trade, firm, or product names is for descriptive purposes only and does  
not imply endorsement by the U.S. Government.

## **Data availability**

430 All data are published as appendices with this article.

## **References**

Arguez, A., Durre, I., Applequist, S., Vose, R. S., Squires, M. F., Yin, X., ... & Owen, T. W. (2012). NOAA's  
1981-2010 US climate normals: Station USW00026616. NOAA National Centers for Environmental Information.  
DOI:10.7289/V5PN93JP Accessed 5-6-2025.

Beck, H. E., Zimmermann, N. E., McVicar, T. R., Vergopolan, N., Berg, A., & Wood, E. F. (2018). Present and future Köppen-Geiger climate classification maps at 1-km resolution. *Scientific data*, 5(1), 1-12. Beget, J. E., & Kargel, J. S. (2008). Volcanoes and permafrost in Bering Land Bridge National Preserve, arctic Alaska. *Alaska Park Sci*, 7, 33-37.

<https://doi.org/10.1038/sdata.2018.214>

Bondre, N. R., & Hart, W. K. (2008). Morphological and textural diversity of the Steens Basalt lava flows, Southeastern Oregon, USA: implications for emplacement style and nature of eruptive episodes. *Bulletin of Volcanology*, 70(8), 999-1019. <https://doi.org/10.1007/s00445-007-0182-x>

Colinvaux, P. A. (1962). The environment of the Bering land bridge. Duke University.

Deschamps, A., Grigné, C., Le Saout, M., Soule, S. A., Allemand, P., Van Vliet-Lanoë, B., & Floc'h, F. (2014). Morphology and dynamics of inflated subaqueous basaltic lava flows. *Geochemistry, Geophysics, Geosystems*, 15(6), 2128-2150.

<https://doi.org/10.1002/2014GC005274>

Downs, D. T., Champion, D. E., Clyne, M. A., & Muffler, L. P. (2021). A multidisciplinary investigation into the eruptive style, processes, and duration of a Cascades back-arc tholeiitic basalt: A case study of the Brushy Butte flow field, northern California, United States. *Frontiers in Earth Science*, 9, 639459.

<https://doi.org/10.3389/feart.2021.639459>

Duraiswami, R. A., Bondre, N. R., Dole, G., Phadnis, V. M., & Kale, V. S. (2001). Tumuli and associated features from the western Deccan Volcanic Province, India. *Bulletin of Volcanology*, 63(7), 435-442.

<https://doi.org/10.1007/s004450100160>

Dzurisin, D., Lockwood, J. P., Casadevall, T. J., & Rubin, M. (1995). The Uwekahuna Ash Member of the Puna Basalt: product of violent phreatomagmatic eruptions at Kilauea volcano, Hawaii, between 2800 and 2100±14C years ago. *Journal of Volcanology and Geothermal Research*, 66(1-4), 163-184. [https://doi.org/10.1016/0377-0273\(94\)00062-1](https://doi.org/10.1016/0377-0273(94)00062-1)

Edwards, B. R., Belousov, A., & Belousova, M. (2014). Propagation style controls lava–snow interactions. *Nature Communications*, 5(1), 5666. <https://doi.org/10.1038/ncomms6666>

Edwards, B. R., Belousov, A., Belousova, M., & Melnikov, D. (2015). Observations on lava, snowpack and their interactions during the 2012–13 Tolbachik eruption, Klyuchevskoy Group, Kamchatka, Russia. *Journal of Volcanology and Geothermal Research*, 307, 107-119. <https://doi.org/10.1016/j.jvolgeores.2015.08.010>

Fenton, C. R., & Niedermann, S. (2014). Surface exposure dating of young basalts (1–200 ka) in the San Francisco volcanic field (Arizona, USA) using cosmogenic <sup>3</sup>He and <sup>21</sup>Ne. *Quaternary Geochronology*, 19, 87-105. <https://doi.org/10.1016/j.quageo.2012.10.003>

Freundt, A., & Schmincke, H. U. (1995). Eruption and emplacement of a basaltic welded ignimbrite during caldera formation on Gran Canaria. *Bulletin of Volcanology*, 56(8), 640-659. <https://doi.org/10.1007/bf00301468>

Griffiths, R. W. (2000). The dynamics of lava flows. *Annual review of fluid mechanics*, 32(1), 477-518. <https://doi.org/10.1146/annurev.fluid.32.1.477>

Harris, A. J., & Rowland, S. (2001). FLOWGO: a kinematic thermo-rheological model for lava flowing in a channel. *Bulletin of Volcanology*, 63(1), 20-44. <https://doi.org/10.1007/s004450000120>

Head III, J. W., & Wilson, L. (1986). Volcanic processes and landforms on Venus: Theory, predictions, and observations. *Journal of Geophysical Research: Solid Earth*, 91(B9), 9407-9446. <https://doi.org/10.1029/jb091ib09p09407>

Heineke, Caroline, Samuel Niedermann, Ralf Hetzel, and Cüneyt Akal. "Surface exposure dating of Holocene basalt flows and cinder cones in the Kula volcanic field (Western Turkey) using cosmogenic <sup>3</sup>He and <sup>10</sup>Be." *Quaternary Geochronology* 34 (2016): 81-91. <https://doi.org/10.1016/j.quageo.2016.04.004>

Herzschuh, U., Böhmer, T., Chevalier, M., Hébert, R., Dallmeyer, A., Li, C., ... & Zheng, Z. (2023). Regional pollen-based Holocene temperature and precipitation patterns depart from the Northern Hemisphere mean trends. *Climate of the Past*, 19(7), 1481-1506.  
<https://doi.org/10.5194/cp-19-1481-2023>

Hirashima, K. (1952). Rate of cooling of lava flows. In *Highway Research Board Proceedings* (Vol. 31).  
<https://onlinepubs.trb.org/Onlinepubs/hrbproceedings/31/31-018.pdf>

Hopkins, D. M. (1959). History of Imuruk Lake, Seward Peninsula, Alaska. *Geological Society of America Bulletin*, 70(8), 1033-1046.  
[https://doi.org/10.1130/0016-7606\(1959\)70\[1033:HOILSP\]2.0.CO;2](https://doi.org/10.1130/0016-7606(1959)70[1033:HOILSP]2.0.CO;2)

Hopkins, D. M. (1963). Geology of the Imuruk Lake area, Seward Peninsula, Alaska (No. 1141-C). US Govt. Print. Off. <https://doi.org/10.3133/b1141c>

Hopkins, D. M. (1988). The Espenberg Maars; a Record of Explosive Volcanic Activity in the Devil Mountain-Cape Espenberg Area, Seward Peninsula, Alaska. National Park Service, Alaska Regional Office.

Iezzi, G., Mollo, S., Ventura, G., Cavallo, A., & Romano, C. (2008). Experimental solidification of anhydrous latitic and trachytic melts at different cooling rates: the role of nucleation kinetics. *Chemical Geology*, 253(3-4), 91-101. <https://doi.org/10.1016/j.chemgeo.2008.04.008>

Johnson DM, Hooper PR, Conrey RM (1999) XRF analysis of rocks and minerals for major and trace elements on a single low dilution Li-tetraborate fused bead. *Adv X-ray Anal* 41:843-867

Kauahikaua, J., Sherrod, D. R., Cashman, K. V., Heliker, C., Hon, K., Mattox, T. N., & Johnson, J. A. (2003). Hawaiian lava-flow dynamics during the Puu Oo-Kupaianaha eruption: A tale of two decades. *USGS Prof. Paper-1676*, 63-88. <https://doi.org/10.3133/pp1676>

Kaufman, D. S., & Hopkins, D. M. (1985). Late Cenozoic radiometric dates, Seward and Baldwin Peninsulas, and adjacent continental shelf, Alaska (No. 85-374). US Geological Survey. <https://doi.org/10.3133/ofr85374>

Keszthelyi, L., & Denlinger, R. (1996). The initial cooling of pahoehoe flow lobes. *Bulletin of Volcanology*, 58, 5-18. <https://doi.org/10.1007/s004450050121>

Keszthelyi, L., Harris, A. J., & Dehn, J. (2003). Observations of the effect of wind on the cooling of active lava flows. *Geophysical Research Letters*, 30(19). <https://doi.org/10.1029/2003GL017994>

Knaack C, Cornelius S, Hooper PR (1994) Trace element analyses of rocks and minerals by ICP-MS. *Geoanalytical Laboratory Wash State Univ* 2: 18

Lal, D. (1991). The present scope of the field of terrestrial cosmogenic nuclides. *Current Science*, 744-751.

Lescinsky, D. T., & Fink, J. H. (2000). Lava and ice interaction at stratovolcanoes: use of characteristic features to determine past glacial extents and future volcanic hazards. *Journal of Geophysical Research: Solid Earth*, 105(B10), 23711-23726. <https://doi.org/10.1029/2000JB900214>

Macdonald, G. A. (1953). Pahoehoe, aa, and block lava. *American Journal of Science*, 251(3), 169-191.

Marchetti, D. W., Hynke, S. A., & Cerling, T. E. (2014). Cosmogenic <sup>3</sup>He exposure ages of basalt flows in the northwestern Payún Matru volcanic field, Mendoza Province, Argentina. *Quaternary Geochronology*, 19, 67-75. <https://doi.org/10.1016/j.quageo.2012.10.004>

Marcucci, E. C., Hamilton, C. W., & Herrick, R. R. (2017). Remote sensing evidence of lava-ground ice interactions associated with the Lost Jim flow, Seward Peninsula, Alaska. *Bulletin of Volcanology*, 79, 1-18. <https://doi.org/10.1007/s00445-017-1176-y>

Marrero, S. M., Phillips, F. M., Borchers, B., Lifton, N., Aumer, R., & Balco, G. (2016a). Cosmogenic nuclide systematics and the CRONUScale program. *Quaternary Geochronology*, 31, 160-187.

<https://doi.org/10.1016/j.quageo.2015.09.005>

Marrero, S. M., Phillips, F. M., Caffee, M. W., & Gosse, J. C. (2016b). CRONUS-Earth cosmogenic  $^{36}\text{Cl}$  calibration. *Quaternary Geochronology*, 31, 199-219.

<https://doi.org/10.1016/j.quageo.2015.10.002>

Marrero, S. M., Phillips, F. M., Caffee, M., & Gosse, J. (2021). Corrigendum to "CRONUS-earth cosmogenic  $^{36}\text{Cl}$  calibration"[*Quat. Geochronol.* 31 (2016) 199-219]. *Quaternary Geochronology*, 61, 101130.

<https://doi.org/10.1016/j.quageo.2020.101130>

Mee, K., Tuffen, H. and Gilbert, J.S. 2006. Snow-contact volcanic facies and their use in determining past eruptive environments at Nevados de Chillán volcano, Chile. *Bulletin of Volcanology*, 68, 363-376.

<https://doi.org/10.1007/s00445-005-0017-6>

Mukasa, S. B., Andronikov, A. V., & Hall, C. M. (2007). The  $^{40}\text{Ar}/^{39}\text{Ar}$  chronology and eruption rates of Cenozoic volcanism in the eastern Bering Sea Volcanic Province, Alaska. *Journal of Geophysical Research: Solid Earth*, 112(B6). <https://doi.org/10.1029/2006JB004452>

Nichols, A. R. L., Potuzak, M., & Dingwell, D. B. (2009). Cooling rates of basaltic hyaloclastites and pillow lava glasses from the HSDP2 drill core. *Geochimica et Cosmochimica Acta*, 73(4), 1052-1066.

<https://doi.org/10.1016/j.gca.2008.11.023>

Nye CJ, Begét JE, Layer PW, Mangan MT, McConnell VS, McGimsey RG, Miller TP, Moore RB, Stelling PL (2018) Geochemistry of some quaternary lavas from the Aleutian arc and Mt. Wrangell: Alaska Division of Geological & Geophysical Surveys Raw Data File 2018–1, 29 p., <https://doi.org/10.14509/29843>

Orr, T. R., Coombs, W. M., Rader, E., & Larsen, J. (2025). Does the Lost Jim flow (Alaska) really preserve evidence of interaction with permafrost?. *Journal of Volcanology and Geothermal Research*, 108347.

<https://doi.org/10.1016/j.jvolgeores.2025.108347>

Oze, C., & Winter, J. D. (2005). The occurrence, vesiculation, and solidification of dense blue glassy pahoehoe. *Journal of Volcanology and Geothermal Research*, 142(3-4), 285-301.

<https://doi.org/10.1016/j.jvolgeores.2004.11.008>

Parmelee, D. E., Kyle, P. R., Kurz, M. D., Marrero, S. M., & Phillips, F. M. (2015). A new Holocene eruptive history of Erebus volcano, Antarctica using cosmogenic <sup>3</sup>He and <sup>36</sup>Cl exposure ages. *Quaternary Geochronology*, 30, 114-131.

<https://doi.org/10.1016/j.quageo.2015.09.001>

Patrick, M. R., Dehn, J., & Dean, K. (2004). Numerical modeling of lava flow cooling applied to the 1997 Okmok eruption: Approach and analysis. *Journal of Geophysical Research: Solid Earth*, 109(B3).

<https://doi.org/10.1029/2003jb002537>

Rader, E., Ackiss, S., Sehlke, A., Bishop, J., Orrill, B., Odegaard, K., ... & Doloughan, A. (2022). Average VNIR reflectance: A rapid, sample-free method to estimate glass content and crystallinity of fresh basaltic lava. *Icarus*, 383, 115084.

<https://doi.org/10.1016/j.icarus.2022.115084>

Reeder, A., Rader, E., & Bishop, J. (2024). Glass, crystallinity, and VNIR reflectance from vent to margin at Jordan Craters, OR USA. *Journal of Volcanology and Geothermal Research*, 447, 108035.

<https://doi.org/10.1016/j.jvolgeores.2024.108035>

Rowland, S. K., Harris, A. J., & Garbeil, H. (2004). Effects of Martian conditions on numerically modeled, cooling-limited, channelized lava flows. *Journal of Geophysical Research: Planets*, 109(E10).

<https://doi.org/10.1029/2004je002288>

Sage, L. L. (2000). A Study of Dense, Glassy Flows: Dense Pahoehoe Lava Flows From Kilauea Volcano, Hawaii. *McNair Scholars Journal*, 4(1), 5.

Schneider, C. A., Rasband, W. S., & Eliceiri, K. W. (2012). NIH Image to ImageJ: 25 years of image analysis. *Nature Methods*, 9(7), 671–675. [doi:10.1038/nmeth.2089](https://doi.org/10.1038/nmeth.2089)

Stone, J. O. (2000). Air pressure and cosmogenic isotope production. *Journal of Geophysical Research: Solid Earth*, 105(B10), 23753-23759.  
<https://doi.org/10.1029/2000JB900181>

Tanaka, K. L., Skinner, J. A., Dohm, J. M., Irwin, R. P., Kolb, E. J., Fortezzo, C. M., ... & Hare, T. M. (2014). Geologic map of Mars (Vol. 3292). Astrogeology Research Program (USGS). <https://doi.org/10.3133/sim3292>

United States, US Department of Agriculture, Natural Resource Conservation Service, National Water and Climate Center. (2024, February 29). *Air and Water Database*. Water and Climate Information System. <https://wcc.sc.egov.usda.gov/nwcc/site?sitenum=986>

Vazquez, J. A., & Woolford, J. M. (2015). Late Pleistocene ages for the most recent volcanism and glacial-pluvial deposits at Big Pine volcanic field, California, USA, from cosmogenic <sup>36</sup>Cl dating. *Geochemistry, Geophysics, Geosystems*, 16(9), 2812-2828.  
<https://doi.org/10.1002/2015GC005889>

Vetere, Francesco, Gianluca Iezzi, Harald Behrens, Francois Holtz, Guido Ventura, Valeria Misiti, Andrea Cavallo, Silvio Mollo, and Marcel Dietrich. "Glass forming ability and crystallisation behaviour of sub-alkaline silicate melts." *Earth-science reviews* 150 (2015): 25-44. <https://doi.org/10.1016/j.earscirev.2015.07.001>

Voigt, J. R., Hamilton, C. W., Steinbrügge, G., & Scheidt, S. P. (2021). Surface roughness characterization of the 2014–2015 Holuhraun lava flow-field in Iceland: Implications for facies mapping and remote sensing. *Bulletin of Volcanology*, 83(12), 82. <https://doi.org/10.1007/s00445-021-01499-4>

Waichel, B. L., de Lima, E. F., Lubachesky, R., & Sommer, C. A. (2006). Pahoehoe flows from the central Paraná continental flood basalts. *Bulletin of Volcanology*, 68(7), 599-610. <https://doi.org/10.1007/s00445-005-0034-5>

Wilding, M., Dingwell, D., Batiza, R., & Wilson, L. (2000). Cooling rates of hyaloclastites: applications of relaxation geospeedometry to undersea volcanic deposits. *Bulletin of Volcanology*, 61, 527-536.

<https://doi.org/10.1007/s004450050003>

Wilding, M. C., Webb, S. L., & Dingwell, D. B. (1995). Evaluation of a relaxation geospeedometer for volcanic glasses. *Chemical Geology*, 125(3-4), 137-148.

[https://doi.org/10.1016/0009-2541\(95\)00067-V](https://doi.org/10.1016/0009-2541(95)00067-V)

Wilding, M., Webb, S., Dingwell, D., Ablay, G., & Marti, J. (1996). Cooling rate variation in natural volcanic glasses from Tenerife, Canary Islands. *Contributions to mineralogy and petrology*, 125, 151-160.

<https://doi.org/10.1007/s004100050212>

Zreda, M. G., Phillips, F. M., Kubik, P. W., Sharma, P., & Elmore, D. (1993). Cosmogenic <sup>36</sup>Cl dating of a young basaltic eruption complex, Lathrop Wells, Nevada. *Geology*, 21(1), 57-60.

[https://doi.org/10.1130/0091-7613\(1993\)021<0057:CCDOAY>2.3.CO;2](https://doi.org/10.1130/0091-7613(1993)021<0057:CCDOAY>2.3.CO;2)

Figures:

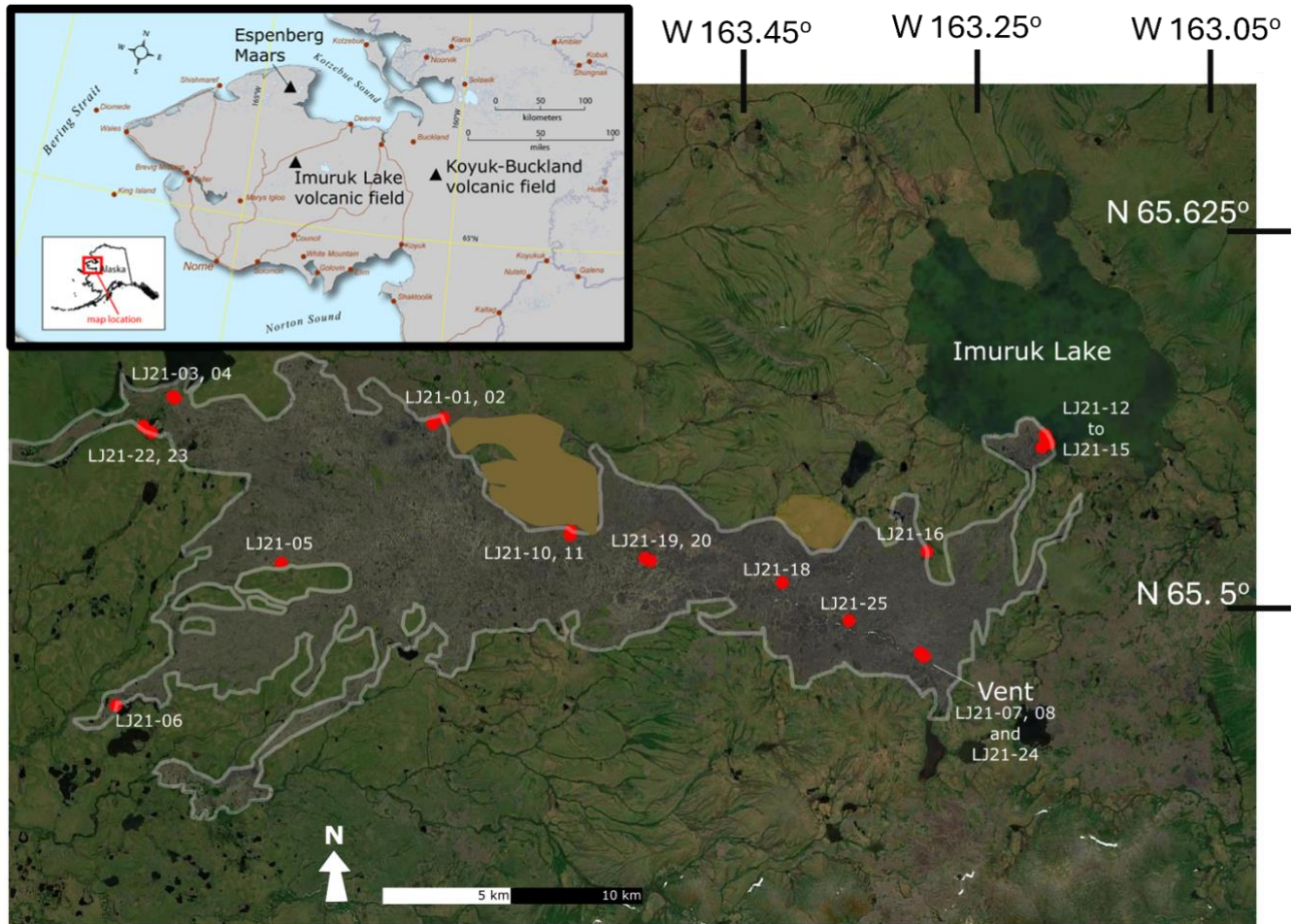


Figure 1. Sample map with Lost Jim flow outlined in grey and Camille flow shaded in orange. Sample locations are shown as red dots with some dots overlapping. Zoomed in maps of these locations can be found in the appendix. Flow is located beneath the word 'Imuruk' in the zoomed out location map reproduced courtesy Schaefer, J. R. G. and the Alaska Volcano Observatory/ Alaska Division of Geological & Geophysical Surveys. Satellite imagery is from Airbus and Maxar Technologies.

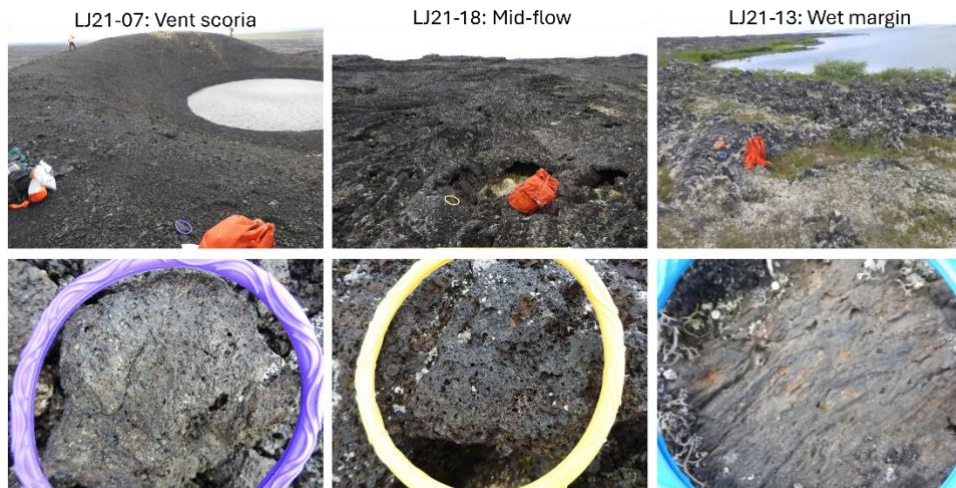
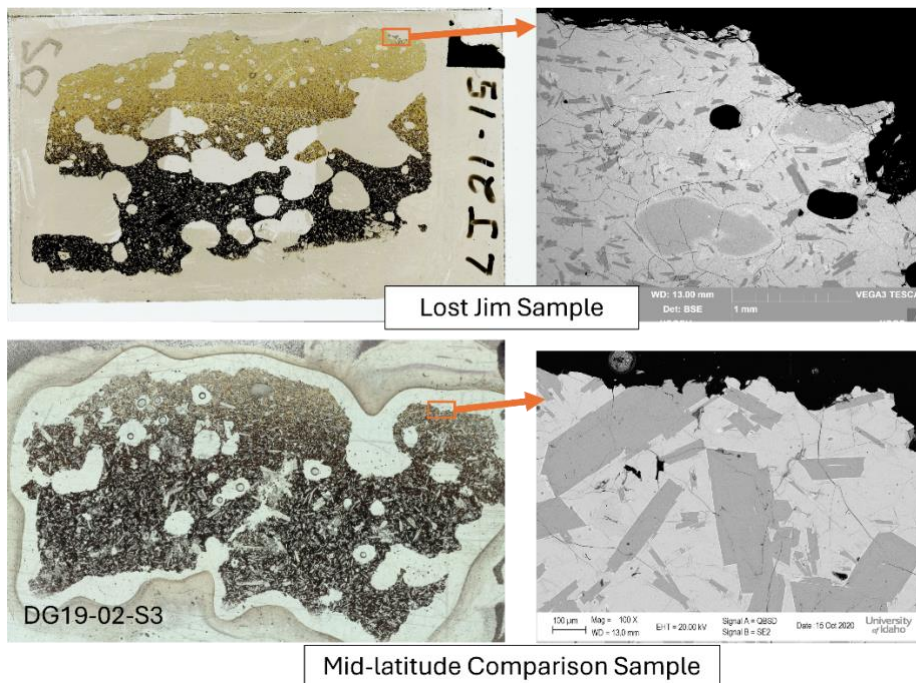
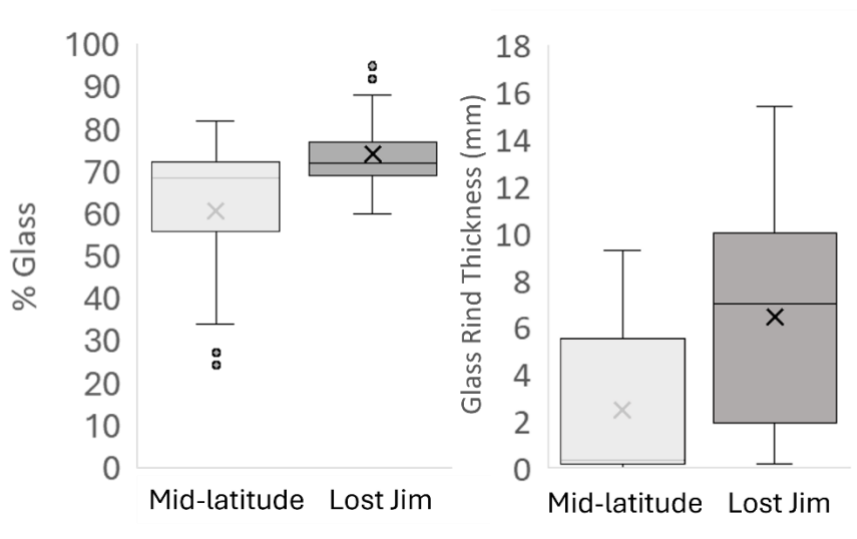


Figure 1: Example photo of vent, mid-flow, and wet margin. Sample rings are 15 cm in diameter. Images of all sampling sites can be found in the appendix.

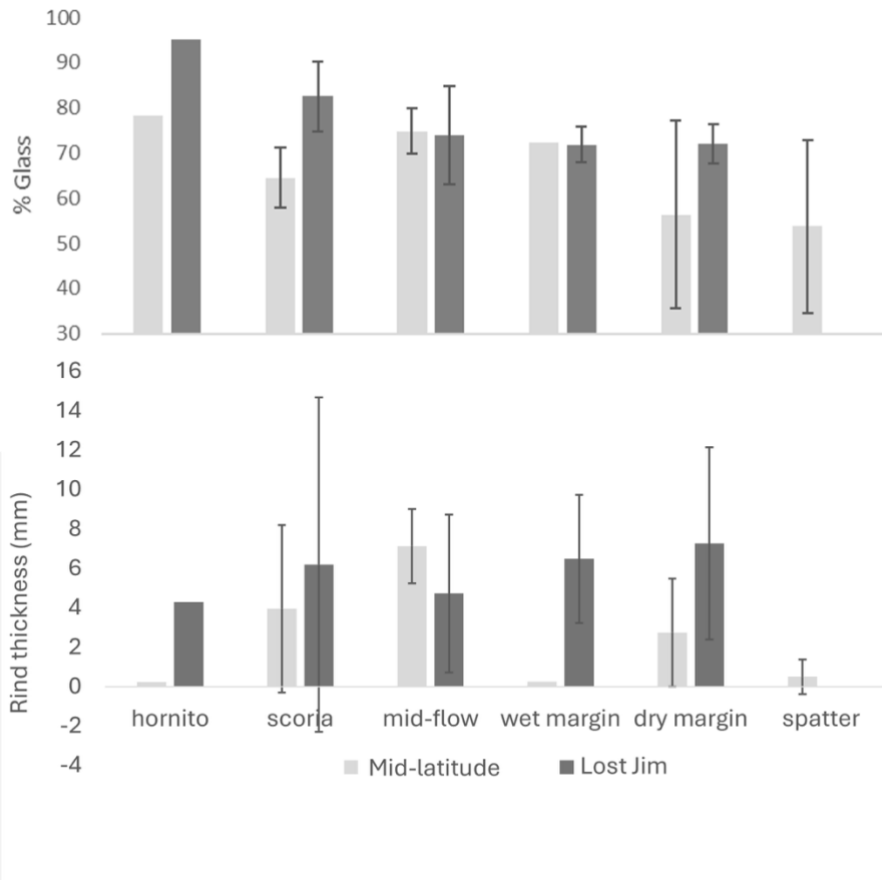


445

Figure 3: Thin section images showing rind thickness and Scanning Electron Microscope (SEM) glass content. Top is Lost Jim flow, bottom is a mid-latitude comparison sample (Devils Garden, Oregon, USA). Images of all Lost Jim thin sections, SEM images, and field photos can be found in the appendix.



450 **Figure 4: Two measures of glassiness from thin sections of the Mid-latitude comparison group (light grey) and the Lost Jim flow samples (dark grey). Plots are box and whisker plots which indicate the average by an 'X' and the median by a line in the middle of the box. Data for these tables are found in Table 1 and 2.**



455 **Figure 5: Two measures of glassiness arranged by emplacement location. Mid-latitude samples are indicated in light grey and Lost Jim in dark grey. The error bars are 1σ. Data (averages for each group) for these graphs are found in Table 4.**